Georgia State University

ScholarWorks @ Georgia State University

Biology Theses

Department of Biology

8-8-2023

Mechanism of Action Of PITM Reduction Of ZIKV Replication In Cell Culture

Oluwatola Femi-Olatunji

Follow this and additional works at: https://scholarworks.gsu.edu/biology_theses

Recommended Citation

Femi-Olatunji, Oluwatola, "Mechanism of Action Of PITM Reduction Of ZIKV Replication In Cell Culture." Thesis, Georgia State University, 2023.
doi: https://doi.org/10.57709/35884162

This Thesis is brought to you for free and open access by the Department of Biology at ScholarWorks @ Georgia State University. It has been accepted for inclusion in Biology Theses by an authorized administrator of ScholarWorks @ Georgia State University. For more information, please contact scholarworks@gsu.edu.

Mechanism of Action Of PI™ Reduction Of ZIKV Replication In Cell Culture

by

Oluwatola Femi-Olatunji

Under the Direction of Julia K. Hilliard, PhD.

A Thesis submitted in Partial Fulfillment of the Requirements for the Degree of

Master of Science

in the College of Arts and Sciences

Georgia State University

2023

ABSTRACT

Zika virus, a single-stranded positive-sense RNA virus belonging to the *Flaviviridae* family, has been linked to a distinct pattern of birth defects and disabilities, as well as Guillain-Barre syndrome in healthy individuals. Proimmune™, free-form amino acids (FFAAP) reduce ZIKV replication by up to 90% in comparison to the mocked-infected cells. The mechanism by which ZIKV replication is reduced is puzzling because blocking intracellular glutathione biosynthesis is still associated with reduced ZIKV replication. Here we provide data generated to test the hypothesis Proimmune™ was sufficient to neutralize ROS, preventing the cell from inducing Oxeiptosis via nrf2 release from KEAP1 the usual innate defense engaged in the presence of pathogen-induced ROS. The data reveal that despite ROS generated post high multiplicity ZIKV infection, Proimmune™ reduces virus replication in the presence of glutathione biosynthesis inhibitors (BSO) and in the absence of ROS upregulation of nrf2-regulated genes that protect cells from excess oxygen free-radicals.

INDEX WORDS: Nrf2, Keap 1, Reactive Oxygen Species, Oxidative stress, Glutathione, Cell toxicity, Cell viability, Oxeiptosis

Copyright by
Oluwatola Femi-Olatunji
2023

Mechanism Of Action Of PI™ Reduction Of ZIKV Replication In Cell Culture

by

Oluwatola Femi-Olatunji

Committee Chair: Julia Hilliard

Committee: Richard Dix

John Houghton

Electronic Version Approved:

Office of Graduate Services

College of Arts and Sciences

Georgia State University

August 2023

DEDICATION

I dedicate this project to God Almighty with whom I have my being and essence. I also dedicate this thesis to my family who supported me to move to the United State from Nigeria to pursue my dreams of learning and practicing quality science.

ACKNOWLEDGEMENTS

My deepest and sincere gratitude goes to my Advisor, Dr. Julia K. Hilliard for her guidance in science, her unique perspective about science and life, has sharpened my view on wonderful science. I am grateful for her profound belief in me as a scientist, her, patience, understanding, and encouragement that helped me through my program. I acknowledge Dr. Richard Dix and Dr. John Houghton who accepted to be part of my thesis committee and have guided me every step of the way with their insightful comments.

I thank the Research scientist, Dr. Judee Nemeno, The senior research scientist, Dr. Irina, Helva Mantugulu for their immense support and always been there when I needed answers to my questions. Furthermore, I appreciate my lab mate, Xiaobei Xu, David Bamisaye, for their technical and emotional support

TABLE OF CONTENTS

LIST OF FIGURES

LIST OF ABBREVIATIONS

I.	AP	Alkaline phosphatase
II.	BCA	Bicinchoninic acid assay
III.	cELISA	Competition ELISA
IV.	DENV	Dengue virus
V.	ELISA	Enzyme-linked immunosorbent assay HRP Horseradish peroxidase
VI.	GSH	Glutathione Synthesis
VII.	JEV	Japanese encephalitis virus
VIII.	KEAP 1	Kelch-like ECH-associated protein 1
IX.	NRF 2	Nuclear factor erythroid 2–related factor 2
X.	RSO	Reactive Oxygen Species
XI.	RT-PCR	Real-time Polymerase Chain Reaction
XII.	SLE	Saint Louis encephalitis
XIII.	WB	Western Blot
XIV.	WN	West Nile virus
XV.	ZIKV	Zika virus
XVI.	P	Immunoprecipation
XVII.	B-ME	β-mercaptothanol

1 INTRODUCTION

Zika virus (ZIKV) is arthropod borne virus that belongs to the *Flavivirus* genus, in the family called *Flaviviridae* that was first discovered in *Aedes africanus* mosquitoes from the same Zika Forest in Uganda in 1947 after being recovered from a feverish rhesus macaque monkey (Dick et al., 1952). The main way that the Zika virus spreads to people is through the bite of an infected Aedes species mosquito (Ae. *aegypti* and Ae. *albopictus*) (Basu and Tumban 2016). These mosquitoes are responsible for transmission of other flaviviruses such as the dengue virus (DENV)and Chikungunya virus, West Nile virus (WNV), Japanese encephalitis virus (JEV), and Yellow Fever virus (YFV). ZIKV can also be transmitted through blood transfusion, organ transplantation, and person-to-person contact that includes sexual interaction, during pregnancy (maternal-fetal vertical transmission. Often, ZIKV infection is asymptomatic or results in a relatively minor sickness with a smooth recovery (Duffy et al.,2019). ZIKV emerged as a global health threat during the 2015 epidemics in South America, with increased virulence, rapid spread, and an association with severe neurological complications like an unanticipated rise in cases of microcephaly in fetuses and newborns and a striking rise in Guillain-Barré syndrome cases (Rasmussen et al., 2016)

The flavivirus genome is a single positive-stranded RNA molecule with a single open reading frame (ORF) with untranslated 5′ and 3′ sections on each side (UTRs). The ORF encodes a polyprotein, which when processed, yields three structural and seven non-structural viral proteins (Rice et al., 1985)

Specifically, the genome of ZIKV is around 10.7 kb long. It only codes for roughly 10.2 kb and contains a single polyprotein that consists of seven nonstructural proteins: NS1, NS2a, NS2b,

NS3, NS4a, NS4b, and NS5 in addition to the three structural proteins capsid (C), pre-membrane (prM), and envelope (E) (Lidenbach et al., 2016). The structural proteins (prM/M and E) are organized with icosahedral symmetry on the surface of the virion, which has a diameter of around 50 nm and contains a nucleocapsid (Bonaldo et al., 2016). Non-structural proteins have crucial roles in host response, polyprotein processing, and genome replication while structural proteins are responsible for the production of the viral particle. (Shi et al., 2016)

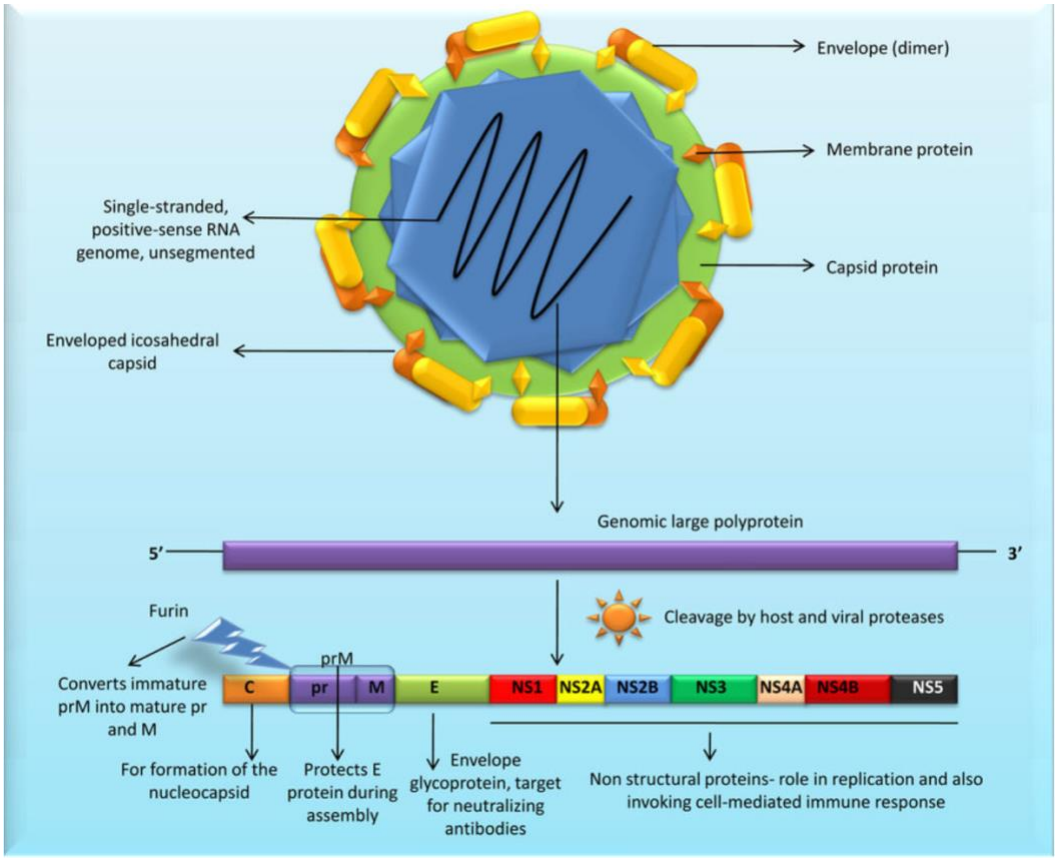

Figure 1:Structure of Zika virus

Source: (Singh et al., 2016)

ZIKV infections have been linked to birth abnormalities, e.g., microcephaly and other neurological conditions that are now generally known as "congenital Zika syndrome."(Del campo et al., 2017). These infections are unique from other congenital virus infections in that pathologic symptoms are predominantly confined to the central nervous system (CNS), causing a spectrum of fetal and birth abnormalities that go beyond microcephaly (Miranda Filho et al.,2016). Fetal brain disruption sequence, a disease that results from partial brain disruption during pregnancy with subsequent collapse of the fetal skull, is one of the most apparent aspects of congenital Zika syndrome.

Research conducted over the past few decades have established the link between oxidative stress and the pathogenesis of various viruses, including flaviviruses. Viral infections usually stimulate ROS production and inhibit antioxidant enzyme levels (Deramaudt et al., 2013)

1.1 RECTIVE OXGYEN SPECIES

Reactive oxygen species, also known as ROS, are oxygen-containing radicals with one or more unpaired electrons that may have been acquired as a result of oxidative stress. (Jakubczyk et al., 2020) High ROS concentrations quickly interact with proteins, lipids, carbohydrates, and nucleic acids, frequently causing irreversible functional changes or even complete destruction.

However, to maintain physiological processes like reproduction, host defense, signal transmission, and gene expression, low quantities of ROS generation are necessary (Droge et al.,2002). ROS control signaling, apoptosis, and growth at the cellular level, at the systems level, ROS enable complex systems like the immune system, brain activity, and blood pressure

regulation. Ray et al. (2012) reported reactive oxygen species (ROS) are produced during mitochondrial oxidative metabolism, as well as in reaction to xenobiotics, cytokines, and bacterial invasion. Data from a number of groups suggest that ROS play a key role in the survival and growth of cells as signaling molecules (Ray et al., 2019)

Reduced ROS concentrations positively influence some viruses promoting replication inside host cells (Balakrishna et al., 2019). Yet, vigorous viral replication generates more ROS, which disturbs the cellular redox equilibrium. As a result of DNA, protein, lipid, and free amino acid damage caused by the excess ROS, infected host cells experience oxidative stress (Halliwell and Gutteridge, 2015). Hence, a potential antiviral target would be Elimination of Oxidative stress or reduction of reactive oxygen species which may be related with the neurological disorders observed in ZIKV infected patients (Ledur et al., 2020).

1.2 GLUTATHIONE SYNTHESIS

Glutathione is a tripeptide made up of three amino acids: cysteine, glycine, and glutamic acid and found in surprisingly high levels of concentrations in cells and serve as an antioxidant molecule in cells (Silvagno et al., 2020). In cells, glutathione can be found in two states: reduced (GSH) and oxidized (GSSG) (Kaplowitz et al., 1985). The two reduced glutathione molecules are joined together at the sulfhydryl groups to form oxidized glutathione. The non-protein thiol protects against oxidative stress that is most prevalent in human. Additionally, GSH plays a significant role in redox signaling, is essential for the detoxification of xenobiotics, and regulates immunological response, fibrogenesis, cell proliferation, and apoptosis. Over 98% of all GSH is in the form of GSH, as the predominant form (Meredith et al.,1989 Yuan et al., 2009). There are

three main GSH reserves in eukaryotic cells. Cellular GSH is primarily found in the cytosol (80–85%), mitochondria (10–15%), and endoplasmic reticulum (5%). (Forman et al., 2009).

The antioxidant function of GSH is accomplished largely by GSH peroxidase (GPx)-catalyzed reactions, which reduces hydrogen peroxide and lipid peroxide as GSH is oxidized to GSSG. GSSG in turn is reduced back to GSH by GSSG reductase at the expense of NADPH, forming a redox cycle.

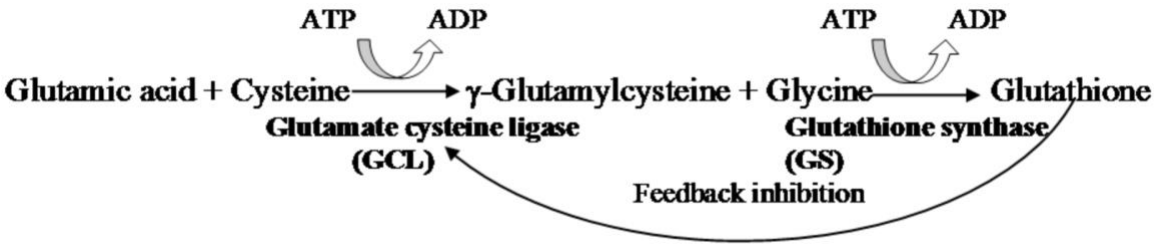

Figure 2: Process of Glutathione Synthesis

The formulation that will be tested in the experiment called FFAAP is a composition of three free-form amino acids i.e., cystine, glycine, and a glutamate source, along with a minute concentration of selenium and found by our group to inhibit Zika virus replication in cell cultures by up to 90% with an ED_{90} of 3 mM (effective dose at which 90% of a dose of Zika virus was inhibited) (Vassiredi et al., 2019).

1.3 SIGNIFICANCE OF STUDY

The composition of FFAAP drives intracellular biosynthesis of glutathione an antioxidant, however, ZIKV inhibition was observed even when we utilized a blockade of intracellular biosynthesis of glutathione. So, the aim this project was to detect the mechanism of action by which FFAAP inhibited ZIKV viral replication in cell culture.

1.4 NRF2: KEAP1 PATHWAY

Higher animals have evolved an additional complex defense mechanisms to fend off the harm that electrophiles and reactive oxygen species (ROS) can cause (Prestera et al. 1993; Primiano et al. 1997) to complement the ancient glutathione defenses conserved as far back as *Archibacteria*. After exposure to electrophiles and ROS, a battery of genes encoding detoxifying and anti-oxidative stress enzymes/proteins is coordinately activated (Beutler et al. 1995; Hayes & Pulford 1995). The antioxidant responsive element (ARE) or electrophile responsive element (EpRE), which functions in the regulatory area of target genes, controls this coordinated response (Rushmore et al. 1991; Friling et al. 1990). ARE/EpRE regulates the genes encoding a subset of drug-metabolizing enzymes, including glutathione S-transferases (GSTs) (Friling et al. 1990) and NAD(P)H-quinone oxidoreductase 1 (NQO1) (Rushmore et al. 1991).
Nuclear factor erythroid 2-related factor 2(NRF2) mediates innate responses to numerous environmental stressors and has a significant impact on intrinsic resistance to oxidative stress. It is a cap'n'collar (CNC) basic-region leucine zipper (bZIP) transcription factor that has the capacity to activate a variety of genes with cytoprotective properties in response to a variety of stimuli, such as redox signaling, inflammation, growth factors, and changes in energy supply (Hayes et al.,2014).

Keap1 is an adapter for Cul3-based E3 ligase and binds Nrf2 extremely tightly to promotes its proteasomal degradation (Itoh et al.,2003; McMachon et al., 2003). The Keap1-Nrf2 complex is broken up by inducers, allowing Nrf2 to go into the nucleus and start the transcription of phase 2 genes (Kobayashi et al.,2004).

In a Keap1-dependent manner, Nrf2 is continuously destroyed under basal conditions by the ubiquitin-proteasome pathway (Sekhar et al. 2002; McMahon et al. 2003; Kobayashi et al. 2004). By heterodimerizing with tiny Maf proteins and activating target genes for cryoprotection via the antioxidant response element (ARE)/electrophile response element (EpRE), Nrf2 can avoid degradation in the presence of electrophiles or ROS (Itoh et al., 2004). Degradation mechanisms, thus, control the levels of Nrf2 protein, and the inducible stabilization of Nrf2 is the fundamental component of the cellular response to oxidative and electrophilic stressors.

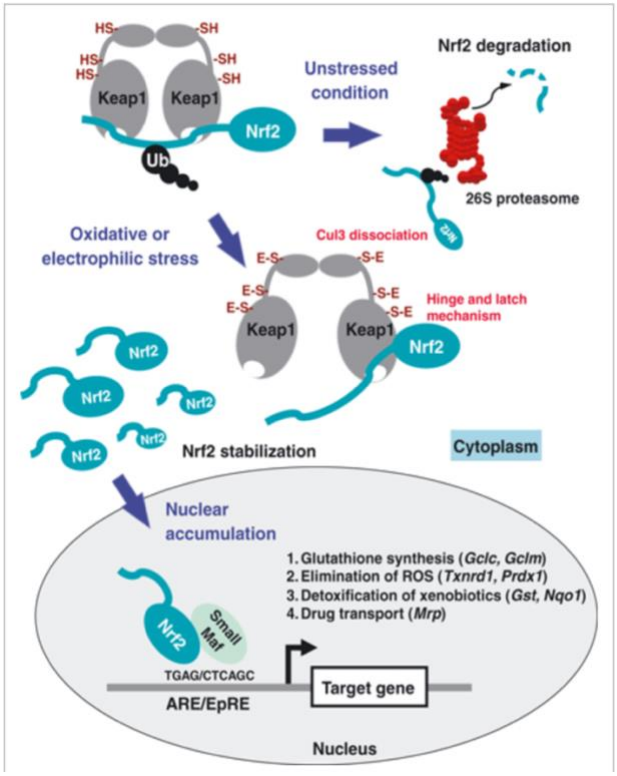

Figure 3:Nrf 2:Keap 1 pathway under stresses and normal condition.

Source: (Taguchi et al., 2011)

2 MATERIALS AND METHODS

2.1 Cell Preparation and Culture

Vero cells (CCL-81) were obtained from ATCC, USA and passaged prior to formation of complete monolayers into DMEM media (Mediatech Inc, USA) supplemented 10% Fetal Serum Bovine (R&D Systems, USA) to ensure dividing cells until ready for experimental manipulation. All cell cultures were maintained in a humidified 37 ^{0}C incubator humidified with 5% CO_2 and air. Cells were passaged for the following experiments using 0.25% trypsin (Sigma, USA) at a ratio of 1:3 once cells reached 90-95 % confluence.

2.2 Cell Treatment with FFAAP

The formulation FFAAP was solubilized and added to 2% DMEM at increasing concentrations 0mM, 2mM, 4mM and 6mM. Twenty T25 Flask (Cell treat, USA) containing kidney cells derived from African Green monkey (ATCC-CCL81, USA) (Passage P10) were cultured in Dulbecco's Modified Eagle's Medium (DMEM) (Mediatech, USA) and grown to a confluency of 95% in DMEM supplemented with 2 % FBS and treated with different concentrations of FFAAP as stated above at 37 °C in 5% CO_2. Treated cells were collected at different time point after FFAAP treatment at 0, 24, 36, 48, 72 and 96 h post treatment, subjected to Cell Titer and Viability Assay™ after centrifugation and resuspension in media and Trypan blue. Cell lysate protein concentration was measured using a Bicinchoninic acid (BCA) protein assay (Thermo Fisher, USA) and SDS-PAGE analysis to cellular detect proteins.

2.3 Cell titer and Viability Assay

The seeded Vero cells were harvested by aspirating the growth media and rinsed with 1xPBS (Mediatech Inc, USA), then incubated in 0.25% trypsin (Mediatech Inc, USA), containing 2.21 mM EDTA, 1X [-] sodium bicarbonate for 2-3 minutes at 37 ^{0}C. After cells were trypsinized from the flask, DMEM was added to inhibit trypsin and centrifuged at 805 x g for 5 mins to collect the pellet, resuspend in fresh media for analysis, and assess cellular morphology and viability by trypan blue staining. Cells (100 ul) were diluted in 900 ul of medium and 100 ul of 4% trypan blue and vortexed properly. An aliquot (10 ul) of cell suspension was carefully loaded between the hemocytometer and matched glass cover slip using a P-20 Pipetman™ and cells that excluded Trypan blue stain (Mediatech, USA) under the microscope were counted to be alive and viable.

2.4 FFAAP-treated ZIKV infected cell lysates preparation.

Monolayers of cells in culture at 95% confluency (derived from adult African green monkey kidneys-**ATCC-CCL81**, USA) (Passage P9) cultured in DMEM (Mediatech, USA) were incubated with ZIKV (PRVABC59 strain at a multiplicity of infection (MOI) of 1 for 1.5h at 37, C. Then, DMEM containing the non- adsorbed virus was removed, and cultured in DMEM supplemented with 2 % FBS treated with increasing concentrations of FFAAP (0mM, 3mM, 4mM) was added and cells were incubated at 37 °C in 5% CO2: 95% air. Infected cells were collected at different time points post viral adsorption at 0, 2, 4, 6, 8, 10, 12, 24, 36, 48, 60 post infection (hpi) and centrifuged at 805 x g for 10 minutes. The protein concentration of ZIKV infected cell lysate was measured using a Bicinchoninic acid (BCA) protein assay (Thermo Fisher, USA). The viral growth titer was assessed by methylcellulose plaque assay on ZIKV infected cell lysate for each time point.

2.5 L-Cystine treated ZIKV infected cell lysates preparation.

Vero cells were infected as previously described with ZIKV (PRABC59 Strain) at a multiplicity of infection (MOI) of 1 for 1h. Then, DMEM containing the non- adsorbed virus was removed, and cultured in DMEM supplemented with 2 % FBS, containing increasing concentrations of L-Cysteine (0 mM, 3 mM, 4 mM) at 37 °C in 5% CO2: 95% air. Infected cells were collected at specific time point after viral adsorption at 2, 4, 6, 8, 10, 12, 24, 36, 48, 60 h post infection (hpi) and centrifuged as described previously. The protein concentration of each ZIKV infected cell lysate harvested was measured using a Bicinchoninic acid (BCA) protein assay (Thermo Fisher, USA). The viral growth was assessed by methylcellulose plaque assay on ZIKV infected cell lysate.

2.6 Bicinchoninic acid (BCA) assay to quantify total proteins levels.

Bovine serum albumin standard (BSA) ampules with a concentration of 1 mg/mL (Thermo Scientific, USA) were diluted and used as a set of protein standards in 1X PBS following the manufacturer's protocol (Thermo Scientific, USA). These were used to generate a standard curve to establish the dynamic range over which infected cell lysate protein concentrations were measured. Lysates prepared with a Halt™ cocktail of protease & Phosphatase Inhibitor (Thermo Scientific, USA) were treated with 10X Tween® 20 and 10X Doc detergent (Sigma-Aldrich, USA) to a final concentration of 1% (v/v), diluted in 1X PBS according to desired dilution ratio. Working Reagents were prepared by mixing 5 mls of BCA Reagent A Bicinchoninic Acid Solution (Sigma, USA) and 100 ul of BCA Reagent B. Copper (II) Sulfate Pentahydrate 4%

Solution (Sigma, USA). An aliquot of (25µl) each standard or unknown sample in triplicate wells of; a flat bottom 96-microplate (Corning Corporation, USA). The specified volume (200µl/ well) of BCA working reagents were added to the utilized wells. The plate was incubated at 37 °C for 30 mins, and the absorbance was measured at $A_{562\ nm}$ using a Bio-Tek plate reader, and the standard curve for this assay plotted. All the protein concentrations were inspected to ensure each unknown was quantified within the range of the standard curve.

2.7 SDS-Polyacrylamide Gel Electrophoresis (SDS-PAGE) and immunoblotting analyses

Laemmli buffer (2X) (Bio-Rad, USA) and 2-mercaptoethanol (Bio-Rad, China) (ratio 20:1) were added to cell lysates at ratio 1:1 after which the samples were boiled at 100^0 C for 5 minutes. Cell lysates are allowed to cool and loaded into stacking gel wells for electrophoresis.

Soluble proteins were separated on a 4% SDS-PAGE gel under reducing conditions by loading prepared cell lysates at same concentration into each of 26-wells of the SDS-PAGE gel, run at 150 Volts, for 60 minutes. Gels were either stained with Coomassie Brilliant Blue or Ponceau Red (EMD Chemicals Inc, England) and then transferred to nitrocellulose membrane (polyvinylidene difluoride membrane (PVDF, Millipore) for immunoblotting. The nitrocellulose containing electrophoretically separated proteins was blocked in blotto (5% Skim milk in BBS) for at least 1h at 37^0 C or overnight at 4^0 C. Membranes were probed with primary antibodies species anti-nrf2 (MBL, Japan), species anti-phospho nrf2, species anti-Keap1, species anti-Actin (Sigma Aldrich) diluted to blotto according to the manufacturer's recommendation at room temperature, and washed 3 times in BBST for 10 min, 5 min, and 5 mins. The nitrocellulose was then probed for I h with species anti- IgG-conjugated to Alkaline phosphate diluted in blotto,

washed 3 times as before and target protein was detected using black vector substrate (Vector Laboratories) made up of, Vector Black Reagent 1, 2 and 3 according to the manufacturer's specifications.

2.8 Methylcellulose Plaque Titration Assay

Confluent Vero cells were infected with a tenfold serial dilution of virus of Hank's Balanced Salt Solution (Gibco HBSS) in 200 ul in 6 well plates. Cells are left to incubate at 37 °C in 5% CO_2, with 15 minutes intermittent swirling of plates. After a 1 h adsorption, the unabsorbed inoculum was removed and 2 mls of maintenance media (DMEM supplemented with 2% FBS) with methylcellulose added to each well. After incubation for 48 h at 37^{o} C, the cells were washed with Phosphate-buffered saline (1X**PBS**), fixed with 100% cold methanol for 20 mins at room temperature, and stained with crystal violet for 10 min at room temperature. Plaques are viewed under the microscope, counted, and values recorded.

2.9 Detection of Reactive Oxygen Species Using Cellrox™ Deep Red™

ROS generation was evaluated by flow cytometry using CellROX™ Deep Red reagent (Invitrogen, USA), which becomes brightly fluorescent when oxidized in cells, allowing sensitive detection of ROS. Vero cells (1.2 X 10^6/mL) were exposed to sodium arsenite (Sigma-Aldrich, USA) (0, 5, 10, and 20 mM/ml) for 7 h to induce ROS after which cells were harvested, rinsed with media, centrifuged at 805 x g for 3 mins, and resuspended in 1 ml of culturing media. Fresh cell ROX solution was made by adding 1 ul of CellROX™ Deep Red reagent in 9 ul DMSO (MP Biomedicals, USA). Resuspended test cells were incubated with 2 ul of Cell ROX

solution away from light at 37^0 C in 5% CO2 for 45-60mins. Incubated cells were then read in the flow cytometry machine at absorption/emission maxima of ~644/665 nm.

2.10 Immunoprecipitation Assay

Infected cell lysate samples were prepared with lysis buffer and mixed with 10 µg of species anti-Nrf 2 antibody (MBL, life science), the reaction volume adjusted to 500 µL with the Cell Lysis Buffer (20 mM Tris HCl pH 8, 137 mM NaCl, 10% Glycerol, 1% Nonidet P-40 (NP-40), 2 mM EDTA) after which the reaction was incubated for 1-2 hours at room temperature or overnight at 4ºC with mixing. Pierce Protein A/G Magnetic Beads (25µl /0.25 ug) (Invitrogen) was added into a 1.5 mL microcentrifuge tubes, washed and 175 µL of Wash Buffer was added to the beads and gently vortexed to mix. The tubes containing the samples were placed into a magnetic stand to collect the beads against the side of the tube after which the supernants were removed and discarded.

The Wash Buffer (Tris-buffered saline (TBS) (1 ml) containing 0.05% Tween-20 Detergent) was added to each sample. The tubes were inverted several times or gently vortexed to mix for 1 minute and beads were collected with magnetic stand. Supernatants were discarded. The antigen samples/antibody mixture was transferred to a 1.5 mL microcentrifuge tube containing pre-washed magnetic beads and incubated at room temperature for 1 hour with mixing. The beads were collected with a magnetic stand and the flow-through removed and saved for analysis. Wash Buffer (500 ul) was added to the tubes and gently mixed. Beads were collected, and supernatants discarded. Wash was repeated twice. Laboratory grade water (500 ul) was added to the tube and gently mixed, the beads on a magnetic stand were collected and supernatant discarded.

Low-pH Elution Buffer (Thermofischer, Illionois) (100 ul) was added to the tubes, which were incubated at room temperature with mixing for 10 minutes. The beads were magnetically separated and supernatants containing target antigen was saved. To neutralize the low pH, Neutralization Buffer (1M Tris; pH 7.5-9) (15 ul) was added for each 100 µL of eluate saved.

2.11 Statistical Analysis: The GraphPad Prism software version 9.0 was used to perform statistical analyses. The differences between two groups (infected and the control groups) or (Treated and the control group(untreated)) were calculated using Student's t-test at 95% confidence, where *P 0.05, **P 0.01 and ***P 0.001. The mean and standard deviation (SD) are used to express the results.

3. RESULT

3.1 Cell counts and viability of Vero cells after the treatment with FFAAP

Cell numbers and cell viability were analyzed by counting live cells that exclude Trypan Blue staining. In the experiment shown in Figure 4, the summarized data show cell numbers versus concentrations of FFAAP used to treat cells. The treated and untreated cells were sampled every 24 hours from the beginning of the experiment (0 h) through 96 h. The results show that statistically similar numbers of live cells were counted up to 72 hours when treatment levels ranged from 0-4 mM FFAAP. There were significantly fewer cells in the group treated with 4 mM FFAAP at 96 hours, which we suggest may be due to the slowing of cell growth in higher concentrations of FFAAP and supported by the observation that in the presence of 6 mM FFAAP, cells did not divide every 24 hours as they did in the treatment groups ranging from 0-4 mM). Data in Figure 5 show that cell viability actually remained high throughout the 96 hour time point in all groups. The effect of FFAAP on cell growth slows but the viability of the cells present remains statistically the same throughout all treatment levels compared to untreated cells. Cells treated with 6 mM FFAAP appear to divide relatively the same as untreated cells up to only 24 hours, with no further cell division occurring. The subsequent experiments presented were performed in the presence of 3 mM FFAAP based on this observation. The interpretation of this observation requires additional future experimentation.

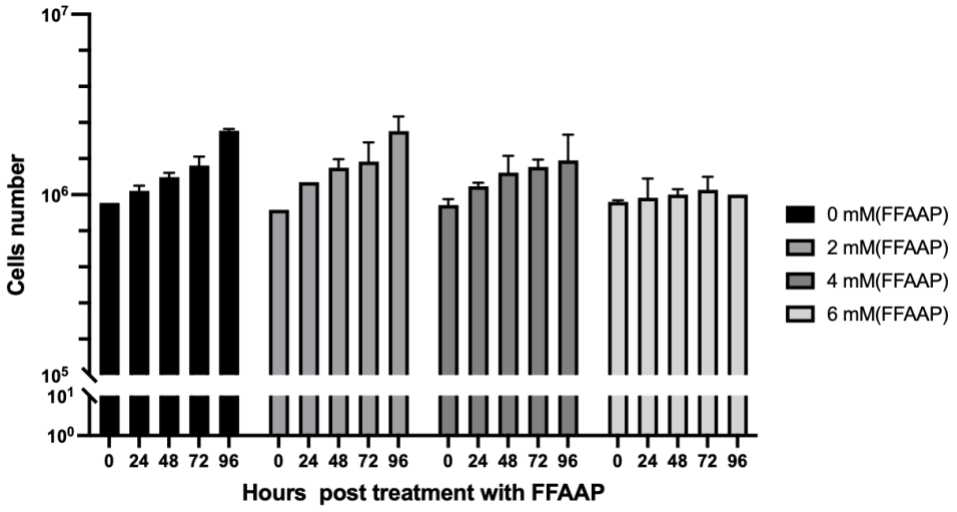

Figure 4:: Vero cell growth over time in culture treated with increasing concentrations of FFAAP

Over time in the presence of increasing concentrations [C] Proimmune™. Standard error of the mean was calculated from triplicate wells of cells while significant effects of the treatment were compared with untreated controls at each time point using one-way Student t-test. Cell doubling time averaged 18-24 hours when cells were grown in DMEM supplemented with either 10% or 2% fetal bovine serum (FBS***)***

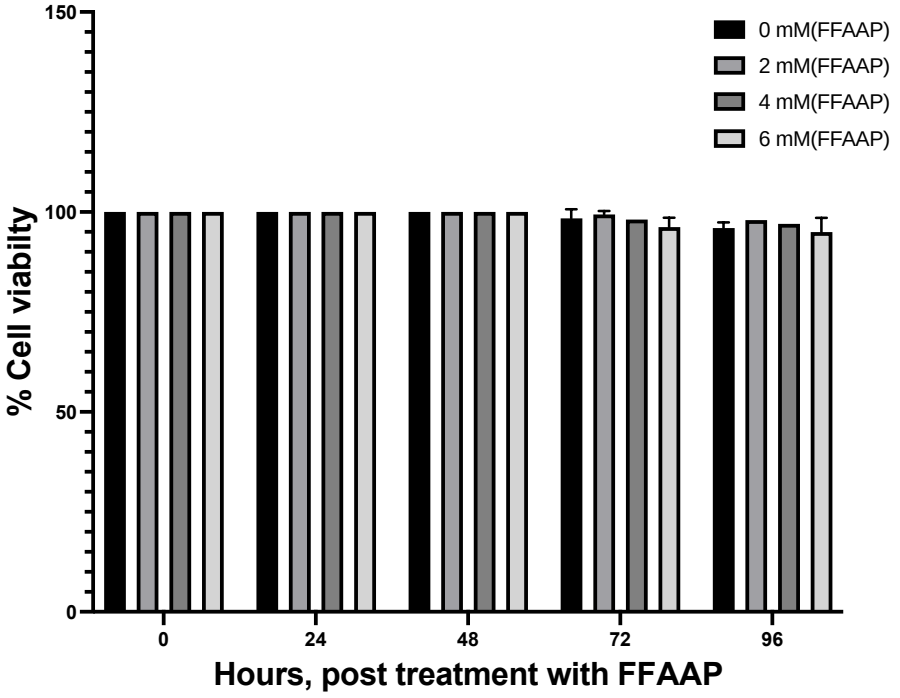

Figure 5:Vero Cell viability after FFAAP treatment at different concentration at specific time point post treatment.

3.2 Vero cells in culture in the presence of FFAAP

Vero cell treated with FFAAP and harvested were tested by the Bicinchoninic acid (BCA) assay.

To further validate the numbers of cells, protein concentration was analyzed. The protein levels would be predicted to increase steadily over time to reflect the growth of the cells in the absence of FFAAP. We noted in Figure 6 that there was a gradual and steady increase in untreated cells up to 72 hours, with a slight, but non-significant decrease at 96 hours, suggesting that these cells in culture reached confluency and ceased dividing probably due to a decrease in media nutrients by 96 hours. Similar observations were seen in the 2 mM treatment group, but the 4 mM treatment group showed erratic protein levels especially noteworthy since cell numbers and viability did not suggest that cells were significantly different from the untreated

controls except at 96 hours. Further analyses of protein levels are needed to validate the results of this experiment.

A.

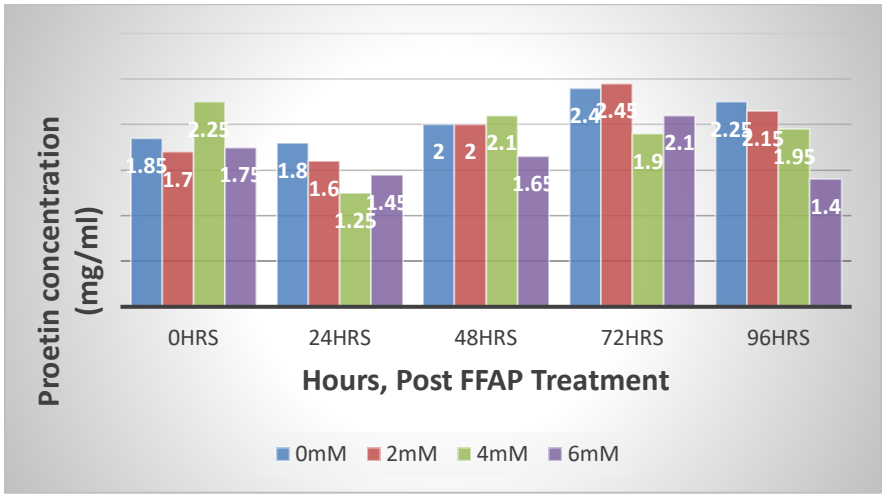

Figure 6:. Protein concentration determination by BCA on Uninfected Vero cells treated with (0mM, 2mM, 4mM, 6mM) concentration of FFAAP and harvested at specific time points (0hrs-96hrs) post treatment.

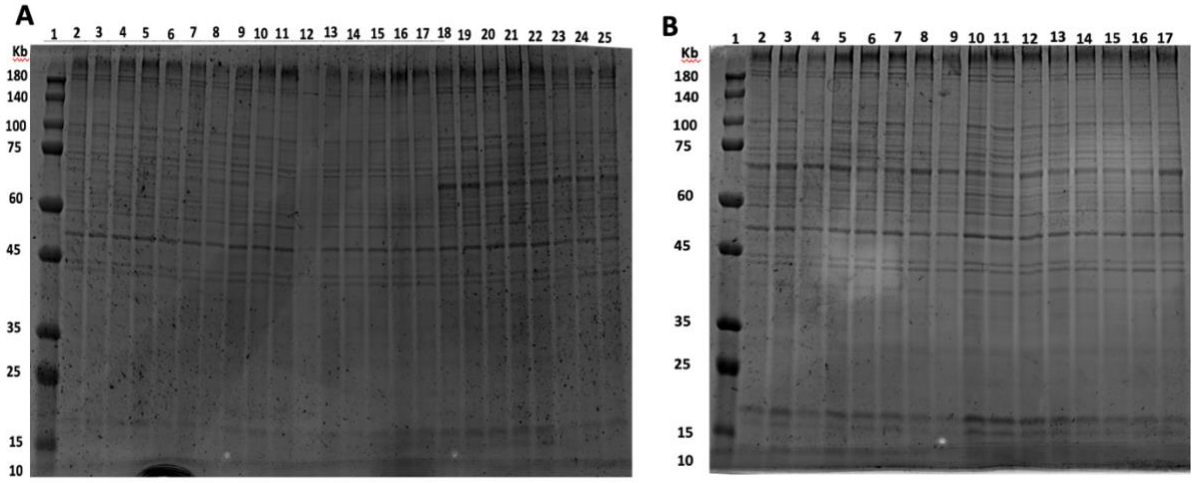

Figure 7:Cellular protein of Vero cell treated with FFAAP.

The Vero cell proteins were detected by staining with Coomassie Blue and rinsing with De staining solution to view with the ChemiDoc imaging MP System (BIO-RAD)

(A) 1- Molecular weight ladder.

0hrs Post Treatment

Lane 2- 0 mM (1) Lane 3- 0 mM (2) Lane 4- 2 mM (1) Lane 5- 2 mM (2)
Lane 6- 4 mM (1) Lane 7- 4 mM (2) Lane 8- 6 mM (1) Lane 9- 6 mM (2)

24hrs Post Treatment
Lane 10- 0 mM (1) Lane 11- 0 mM (2) Lane 12- 2 mM (1) Lane 13- 2 mM (2)
Lane 14- 4 mM (1) Lane 15- 4 mM (2) Lane 16- 6 mM (1) Lane 17- 6 mM (2)

48hrs Post Treatment
Lane 18- 0 mM (1) Lane 19- 0 mM (2) Lane 20- 2 mM (1) Lane 21-2 mM (2)
Lane 22- 4 mM (1) Lane 23- 4 mM (2) Lane 24- 6 mM (1) Lane 25- 6 mM (2)

(B) 1- Molecular weight ladder.
72hrs Post Treatment
Lane 2- 0 mM (1) Lane 3- 0 mM (2) Lane 4- 2 mM (1) Lane 5- 2 mM (2)
Lane 6- 4 mM (1) Lane 7- 4 mM (2) Lane 8- 6 mM (1) Lane 9- 6 mM (2)

96hrs Post Treatment
Lane 10- 0 mM (1) Lane 11- 0 mM (2) Lane 12- 2 mM (1) Lane 13- 2 mM (2)
Lane 14- 4 mM (1) Lane 15- 4 mM (2) Lane 16- 6 mM (1) Lane 17- 6 mM (2)

To determine whether the SDS-PAGE fractionated cell proteins changed visibly with increasing doses of FFAAP treatment over 96 hours, cell profiles were evaluated by visual inspection (Figure 7 a). Load amounts per lane were too low to resolve many bands below ~40 kD, although several bands at ~20 kD and lower were resolved and apparent. Lanes 0-9 show each treatment group at the initiation of this experiment. Untreated cells were observed to have protein profile changes at 24 hours as shown in Lanes 10 and 11. Lanes 12-13 reflect the cell proteins in the 2 mM treatment group, Lanes 14-15 the 4 mM treatment group, and Lanes 16-17 show the 6mM treated cell profiles. Lane 12 indicates a sample load error or a problem with the cells in this duplicated of the 2 mM treatment. Regardless, a ell protein band at ~90 kD fades significantly at 24 hours in all treatment groups (Lanes 10-17), but reappears and remains present from Lanes 18-25. The identity of the protein migrating at this position will be subsequently identified using mass spectroscopy. A similar disappearance of a band at ~70 kD disappears in the 2 mM treatment group and reappears in

more concentrated amounts the 48-hour treatment group at all concentrations of FFAAP. These differences are curious but require further analyses to determine the significance of the appearance and disappearance. In Figure 7b the 72 hours and 96-hour treatment groups are shown. Again, each lane has an adjacent duplicate sample. Visual inspection of each of the duplicate sets generally reveals no major differences between most duplicates or relative load issues with the exception of lane 9. There are some differences in band intensity increasing at ~40 kD, but again additional analyses will be required. Overall, there are no apparent differences in the cell proteins fractionated under denaturing conditions on SDS-PAGE following extended treatment with increasing levels of FFAAP over 96-hours.

3.3 Plaque Assay of Zika infected Vero cells: FFAAP Treated and Untreated Vero cells

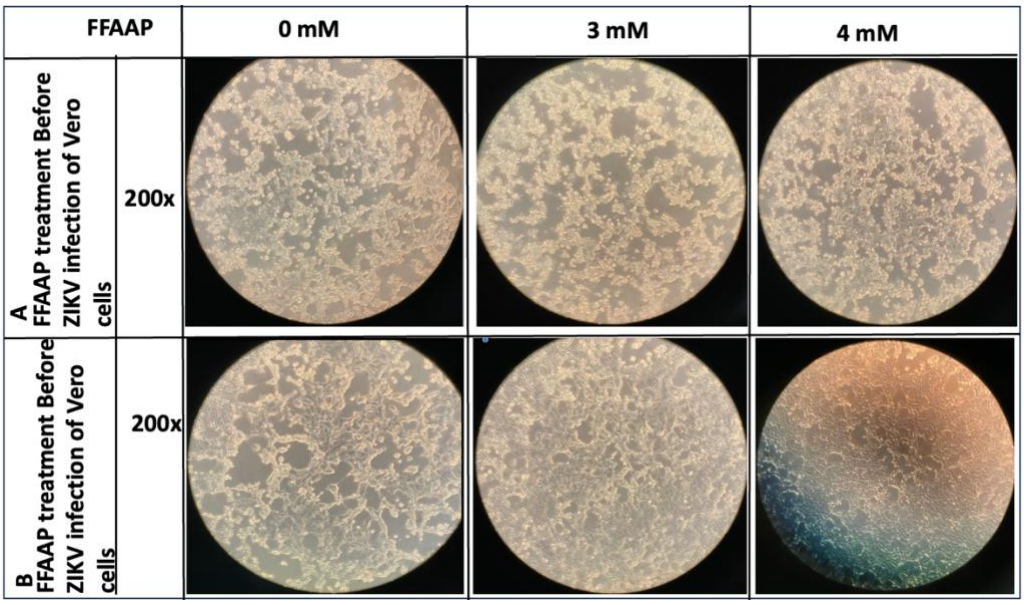

Figure 8::(a)-ZIKV-infected Vero cells at 72 hpi with 24hrs pre-treatment (0 mM, 3 mM, 4 mM FFAAP) before ZKV infection MOI 1. (b) ZIKV-infected Vero cells at 72 hpi with post-treatment (0 mM, 3 mM, 4 mM FFAAP) after ZIKV infection, MOI 1.

The cytopathic effect of virus CPE was accessed by viewing under the microscope. There is more CPE found in infected Vero cells without treatment of FFAAP compared to with treatment of FFAAP regardless of method and time at which cells were treated with FFAAP.

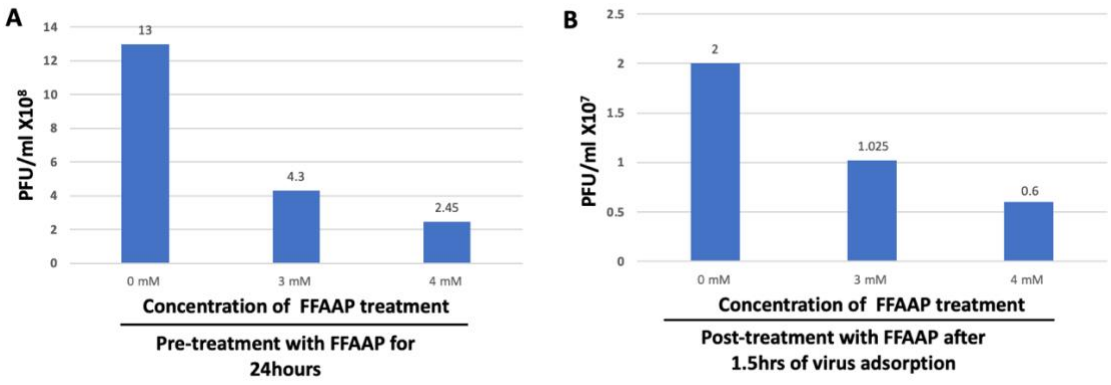

Figure 9:ZIKV replication in treated culture after 72 hours.

The inhibitory concentration of FFAAP (IC_{50}) of ZIKV replication in the Vero cells was determined to be the reciprocal of the virus titer, the higher the dose, the greater the reduction in virus titer over time under the same condition. The high viral replication of ZIKV in a 24hr pre-treated compared to post treatment of ZIKV infected cells could be as a result of the early starvation of Vero cells of Fetal Bovine Serum (2% FBS) for 24 hours for the effective treatment with FFAAP compared to post treatment which had (10%FBS), 24 hours before treatment.

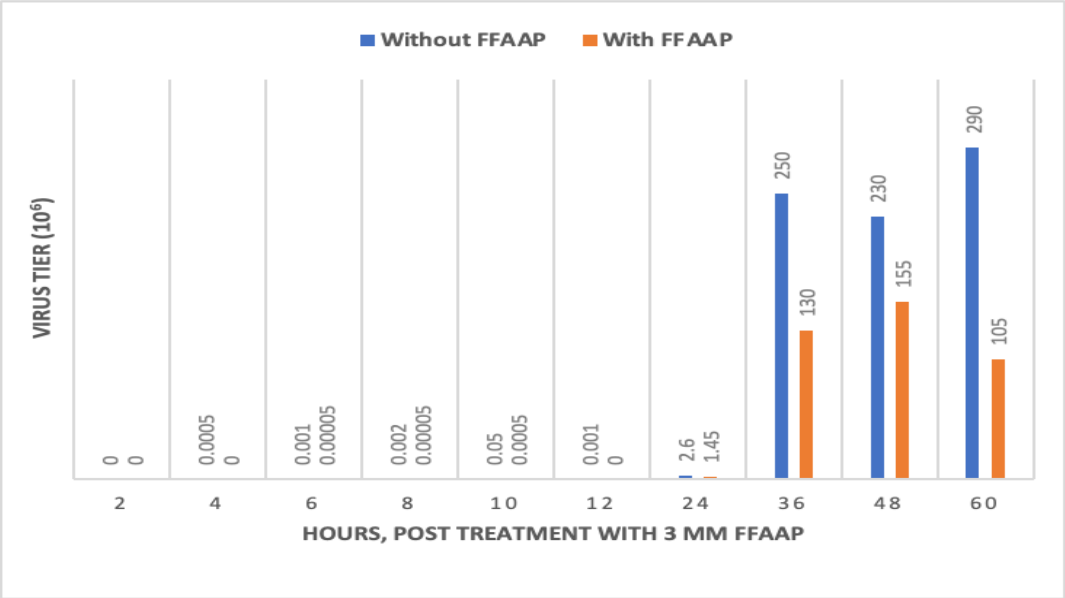

Figure 10:ZIKV Replication in Cells Treated & Untreated with 3mM FFAAP over 60hpi.

(A)

UU= Uninfected: Untreated
UT= Uninfected: Treated
IU= Infected: Untreated
IT= Infected: Treated

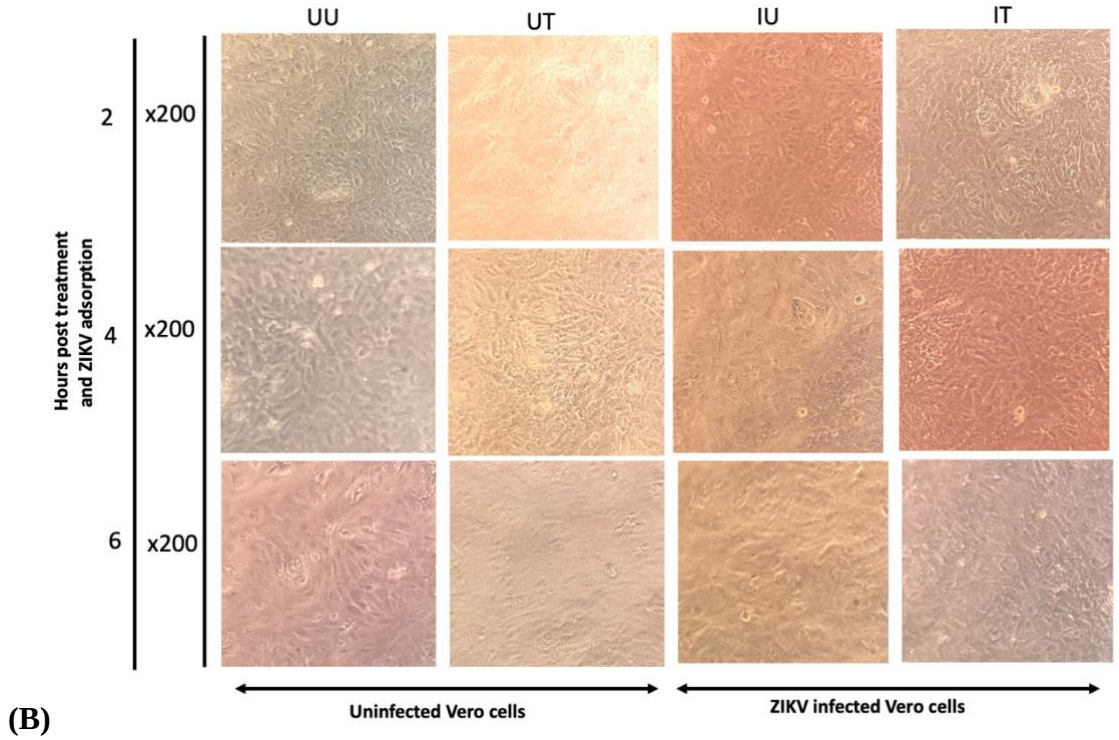
UU
UT
IU
IT
2
x200
4
x200
6
x200
Hours post treatment and ZIKV adsorption
Uninfected Vero cells
ZIKV infected Vero cells

(B)

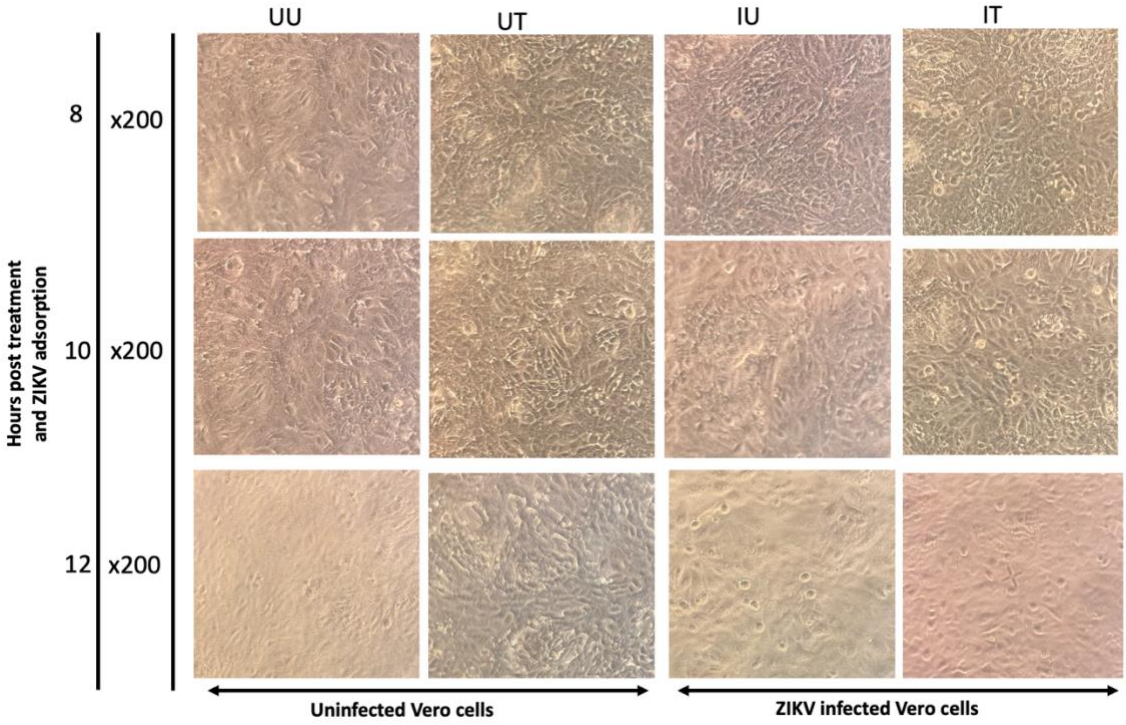
UU
UT
IU
IT
8
x200
10
x200
12
x200
Hours post treatment and ZIKV adsorption
Uninfected Vero cells
ZIKV infected Vero cells

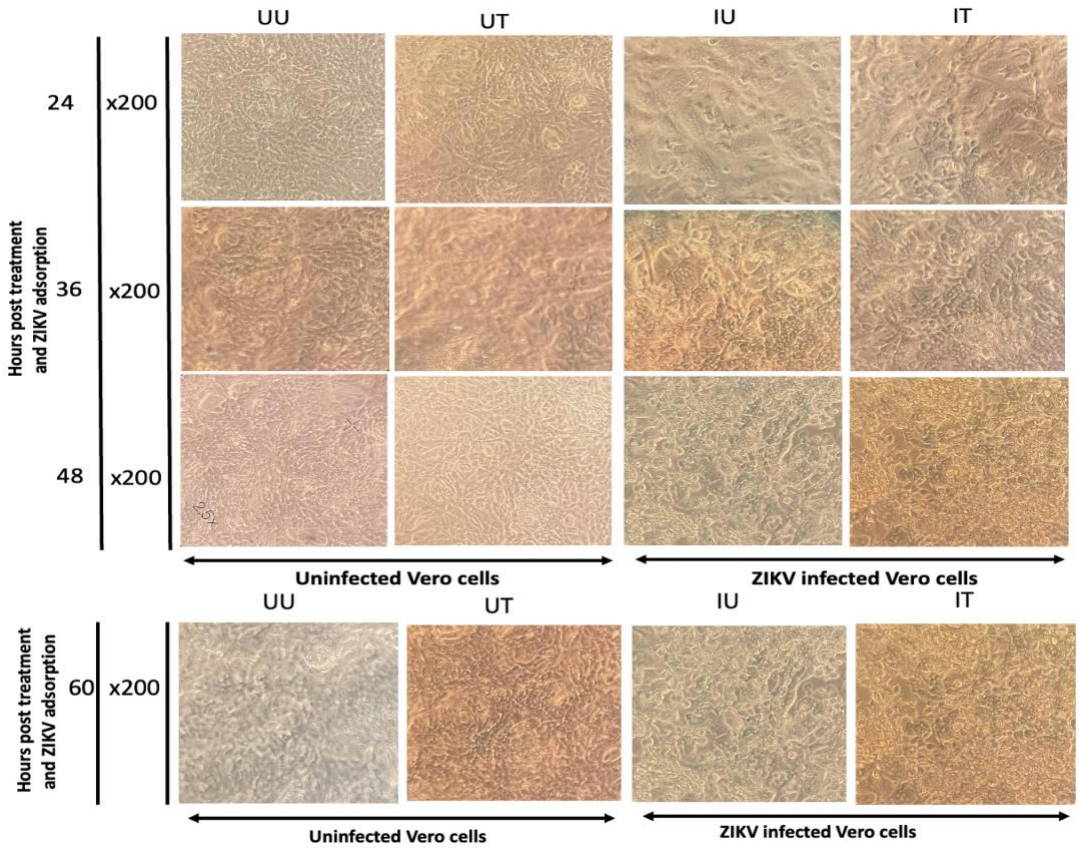

(C)

Figure 11:Cytopathic effect of Zika virus infection in Vero cells through its replication cycle.

Cell growth and ZIKV replication was captures under the Microsoft before harvesting for further analysis to observe the Cytopathic effect (CPE) in correlation to molecular changes in the cells. CPE was observed as a rounded cell foci on the monolayer. starting from 12hpi and was more visible at 36hpi.

3.4 Reactive Oxygen Species measurement with flow cytometry

Vero cells treated with 3mM of FFAAP were compared to non-treated cells and ZIKV infected Vero cells, both treated with FFAAP and untreated respectively. Vero Cells treated with difference concentrations of Sodium Arsenite NaAsO2 were used as positive control to help with gating of the ROS measurement while using the flow cytometry.

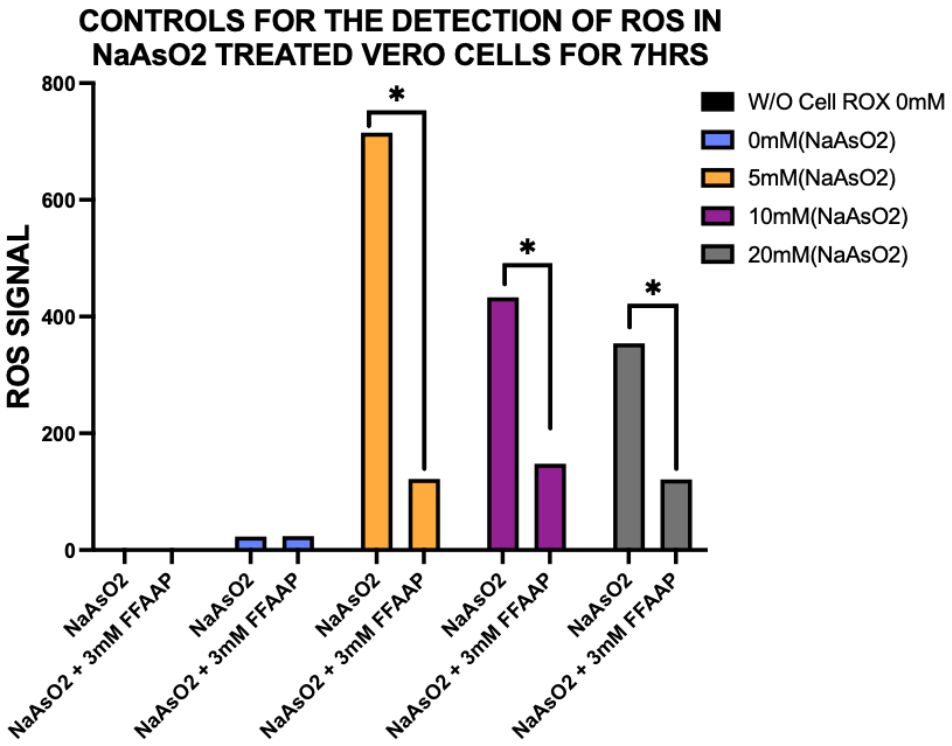

Figure 12:Detection of ROS in Sodium Arsenite (NaAsO2) using CellROX™ Deep Red after 7hours of total incubation.

The treatment with NaAsO2 was used as a positive control to induce ROS signal in the host (Li et al., 2013). After the 7 hours of treatment and one hour of incubation with cell ROX, Vero cells treated with 5mM showed highest ROS signal. Treatment with FFAAP, showed a decrease in ROS signal which showed an effectiveness of the Master antioxidant.

A.

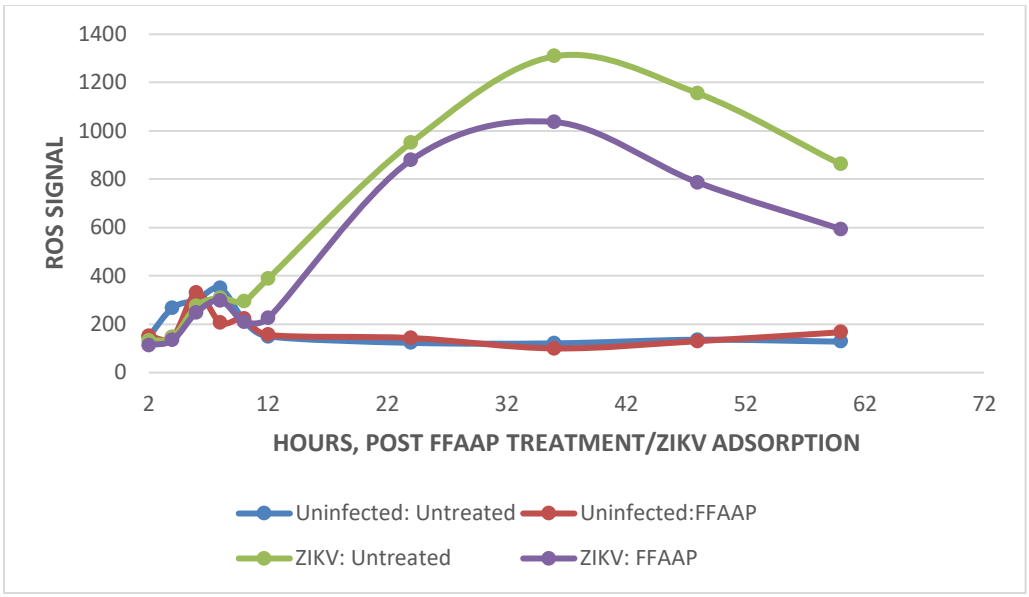
1400
1200
1000
800
600
400
200
0
ROS SIGNAL
2
12
22
32
42
52
62
72
HOURS, POST FFAAP TREATMENT/ZIKV ADSORPTION
Uninfected: Untreated
Uninfected:FFAAP
ZIKV: Untreated
ZIKV: FFAAP

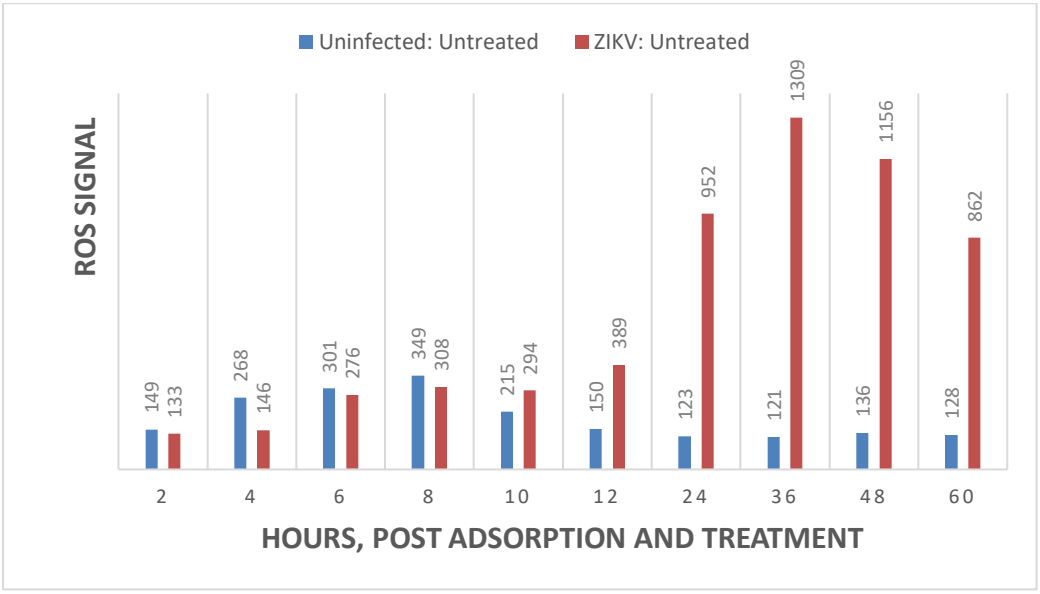
Uninfected: Untreated
ZIKV: Untreated
ROS SIGNAL
149
133
268
146
301
276
349
308
215
294
150
389
123
952
121
1309
136
1156
128
862
2
4
6
8
10
12
24
36
48
60
HOURS, POST ADSORPTION AND TREATMENT

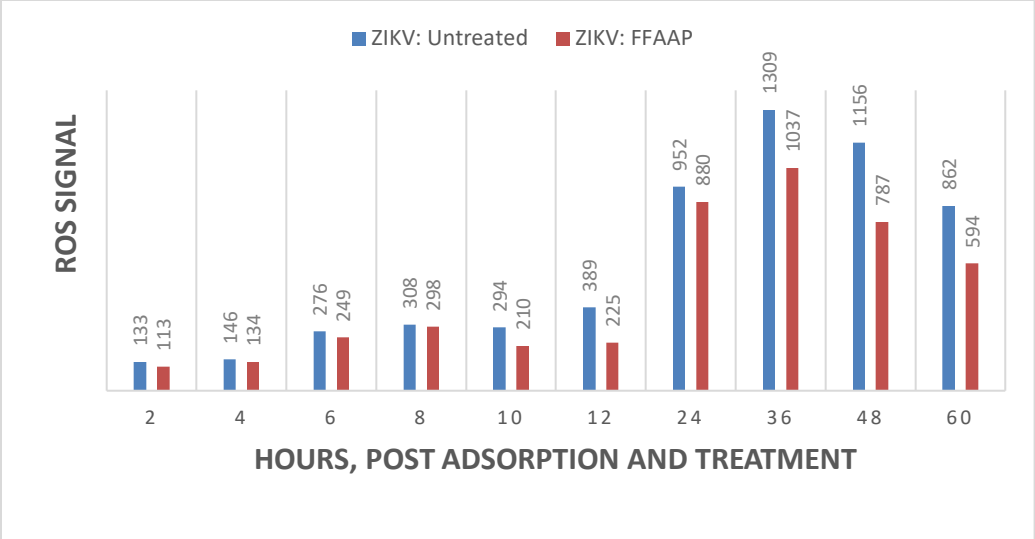
ZIKV: Untreated
ZIKV: FFAAP
ROS SIGNAL
133
113
146
134
276
249
308
298
294
210
389
225
952
880
1309
1037
1156
787
862
594
2
4
6
8
10
12
24
36
48
60
HOURS, POST ADSORPTION AND TREATMENT

D.

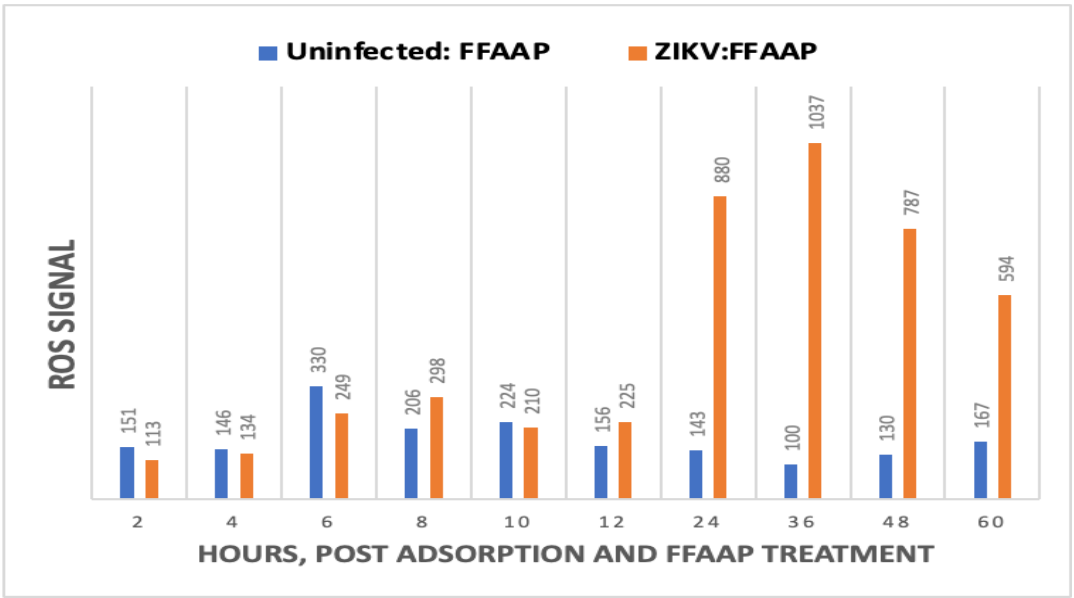
Uninfected: FFAAP
ZIKV:FFAAP
ROS SIGNAL
151
113
146
134
330
249
206
298
224
210
156
225
143
880
100
1037
130
787
167
594
2
4
6
8
10
12
24
36
48
60
HOURS, POST ADSORPTION AND FFAAP TREATMENT

E.

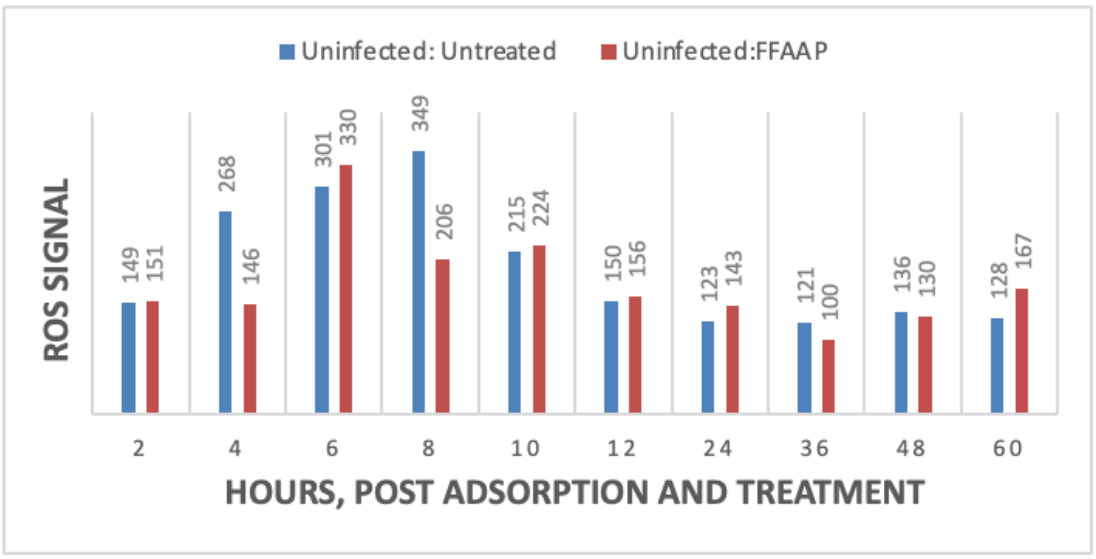

Figure 13: (A.) ROS Production in ZIKV Infected Cells Treated & Untreated. (B.) Effect of ZIKV infection on ROS signal in Vero cells, (C.) Effect of FFAAP on ROS signal on ZIKV infected Vero cells (D) Effect of ZIKV infection on ROS signal in Vero cells in the presence of FFAAP (E) ROS production in uninfected Vero cells Treated and Untreated

ROS was measured at absorption/emission maxima of ~644/665 nm.

Figure 13(b, c, d) was significantly different with p value 0.0363(*) ,0.0120(*) and 0.0455(*) respectively.

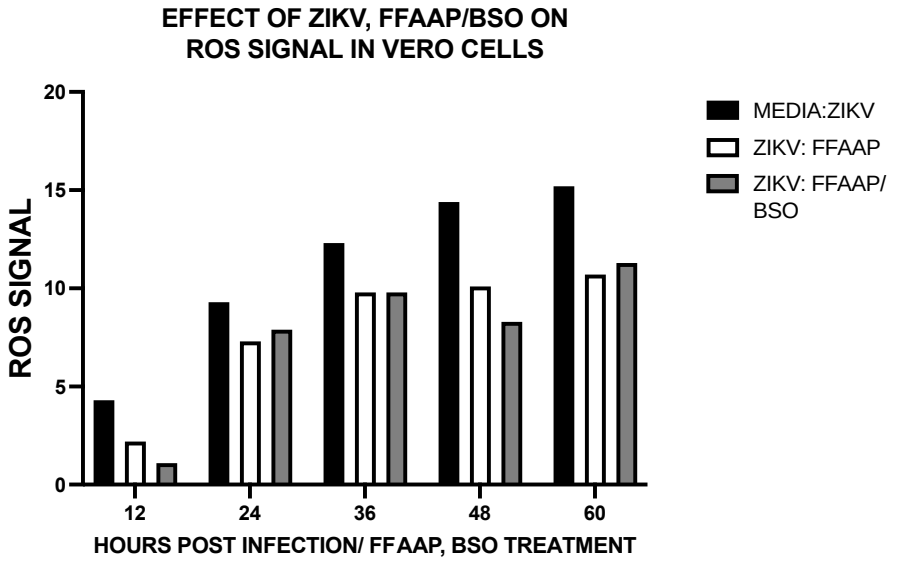

Figure 14:ROS production in FFAAP and Buthionine sulfoximine treated ZIKV infected Vero cells over a period of 60 hours.

3.5 Detection of Nrf2:Keap 1 Pathway using Immunoprecipation and Immunoblotting analysis.

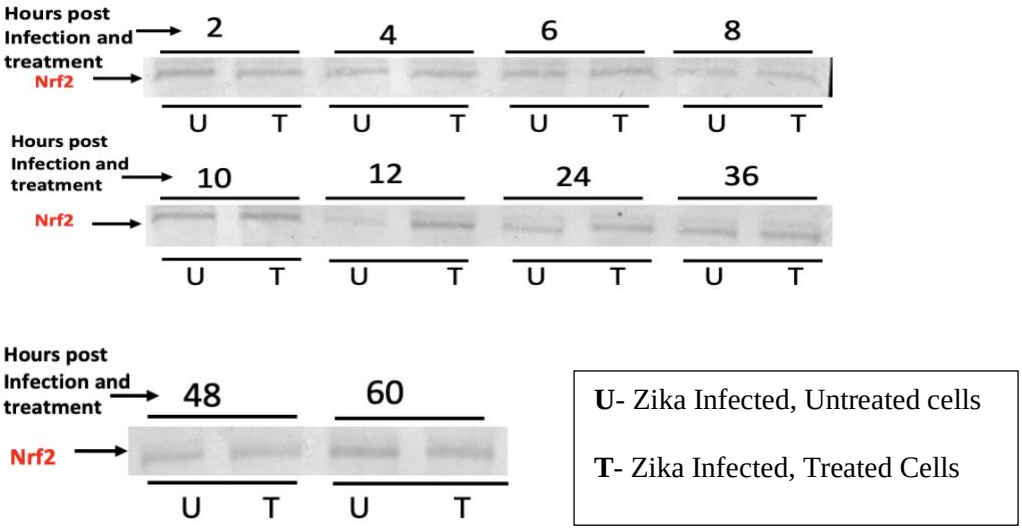

Figure 15:Effect of Zika replication and FFAAP treatment on Nrf2 protein.

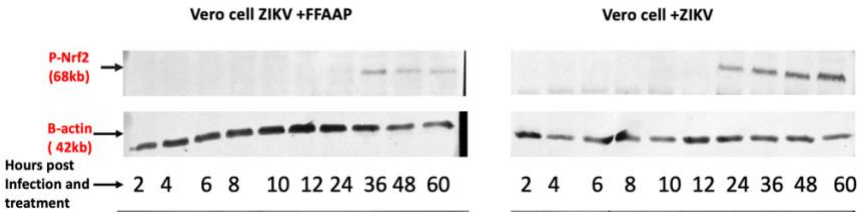

Figure 16: Effect of Zika virus Infection and FFAAP on phosphor Nrf2 and nrf2:keap1 complex.

4 CONCLUSION

Numerous studies have been done on the underlying mechanisms of the Zika virus, yet there is currently no cure for the infection (Munjal et al.,2017). Therefore, it is essential to create powerful medications and vaccinations that can stop the Zika virus to prevent a pandemic.

We investigated the mechanism of action of Zika virus inhibition by FFAAP treatment in Vero cells, where we confirmed the inhibition of Zika virus by the treatment of FFAAP before and after infection at MOI 1.

In our present study, we initially treated Vero cells with different concentrations of FFAAP (0mM, 2mM, 4mM, 6mM) at different time points post-treatment to check the toxicity of FFAAP on the host cells, the virus will grow in, and we found that at the highest concentration (6mM), At 96hours post-treatment, the cells were viable at 98% viability and had increased in cell titer. This shows that the inhibition of the Zika virus in Vero cells was not a result of the death of the host cells but more to do with the inhibition of the virus and its pathway.

After cells were treated with FFAAP before and after infection with ZIKV, it was discovered that treating cells with FFAAP 24 hours before infection increased the inhibition of ZIKV more than treating cells after ZIKV infection.

To detect the mechanism by which FFAAP uses to inhibit ZIKV replication, the Reactive oxygen was measured. Uninfected Vero cells were treated with FFAAP, and untreated were analyzed for ROS signal throughout 60hours compared to infected cells to rule out factors that could induce ROS. We observed a stable low ROS signal in the uninfected cells for 60 hours but observed an increase in ROS signal (Fig. 13B) in infected cells at 12 hours and a sharp increase at 24 hours when CPE was observed (Fig. 11). These results confirmed that ZIKV infection induces ROS (Almeida et al.,2020)

This experiment confirmed that the increase in ROS occurs slowly at the start of virus infection (HPI), rising sharply at 36 hpi & decreasing at 40 hpi. This shows the direct relationship between an Increase in ROS and viral Replication and indicates that although ZIKV Induces ROS, it also flourishes well with an increase in ROS, Independent of the time of Replication or time after infection (Fig 13A), which implicates ROS in the replication of ZIKV .

This showed the non-cytotoxic free-form amino acids (Fig.5) ability to decrease ZIKV replication (Fig. 10) having a positive relationship with ROS production (Fig. 13A).

FFAAP was thought to be able to inhibit ZIKV replication by the glutathione synthesis pathways, but after treating infected cells with FFAAP +BSO, ZIKV replication decreased despite blocking glutathione biosynthesis (Vasireddi et al., 2019). Hence, that hypothesis was ruled out while another pathway of controlling oxidative stress was analyzed. The samples were analyzed for ROS signal, and Zika-infected treated cells with FFAAP and BSO had a decrease in ROS signal despite blocking glutathione biosynthesis (Fig 14) with a reduction in viral compared to untreated cells with Higher ROS With the increase in viral titer, this further confirms the implication of ROS in ZIKV pathogenesis.

Several viruses control ROS levels and enable successful reproduction inside host cells by modifying the Nrf2 pathway (Lee, 2018); hence, to discover the effect of FFAAP on the Nrf 2: keap1 pathway, the cells were probed for Nrf2 and phosphor-Nrf2. ZIKV replication increases ROS but fails to activate nrf2 phosphorylation in the presence of FFAAP by 24 hours compared to untreated ZIKV-infected cells (Fig 17). The increase in ROS aligned with the activation of Nrf 2, although the action of Nrf2 is known to an upregulate antioxidant gene, which is expected to inhibit viral Replication (Saha et al.,2020), this result showed that ZIKV is one of the viruses using the phosphorylation of Nrf2 to its advantage , in its replication (Ramazeni et al., 2018),

although the mechanism is unknown. While phospho-Nrf2 was present at the later part of Replication, Nrf2 was present through the hours of infection in both treated and untreated cells.

Collected Harvest lysate were immunoprecipitated for nrf2 protein and probed for keap1 protein to determine the effect of FFAAP treatment on the nrf2: Keap1 complex, which is known to regulate oxidative stress (Biard et al., 2020) that ZIKV has been known to thrive in (Ramezani et al.,2018). The complex was found prominent in infected cells in the early hours of infection throughout the 60 hours. Nrf2: keap1 was found in the early hours of infection but disappeared in the later hours of infection from 36h hours in untreated cells. This result shows that despite the activation of NrF2 with light intensity, there is the presence of the nrf2; keap1 complex which is implicated in the inhibition of Viral application and known to keep cell homeostasis (Yamamoto et al.,2018).

Taken together, we have shown that the inhibition of ZIKV replication by FFAAP is not by the glutathione pathway but must do more about the ability to reduce the Reactive oxygen Species and keep the Nrf2:Keap1 complex longer. We also found that ZIKV uses the translocation and phosphorylation of Nrf2 in its replication in the host (Ramezani et al., 2018)

Finally, understanding the pathway being exploited by FFAAP in inhibiting ZIKV will be useful in future research since our findings point to the potential for using antioxidants as a cutting-edge therapeutic strategy to treat Zika disease.

REFERENCES

1. Dick, G. W., Kitchen, S. F., & Haddow, A. J. (1952). Zika virus (I). Isolations and serological specificity. *Transactions of the royal society of tropical medicine and hygiene*, *46*(5), 509-520.
2. R. Basu, E. Tumban Zika Virus on a Spreading Spree: what we now know that was unknown in the 1950's
3. Rice, C. M., Lenches, E. M., Eddy, S. R., Shin, S. J., Sheets, R. L., & Strauss, J. H. (1985). Nucleotide sequence of yellow fever virus: implications for flavivirus gene expression and evolution. *Science (New York, N.Y.)*, *229*(4715), 726–733. https://doi.org/10.1126/science.4023707
4. Silvagno, F., Vernone, A., & Pescarmona, G. P. (2020). The Role of Glutathione in Protecting against the Severe Inflammatory Response Triggered by COVID-19. *Antioxidants (Basel, Switzerland)*, *9*(7), 624. https://doi.org/10.3390/antiox9070624
5. Del Campo M, Feitosa IM, Ribeiro EM, Horovitz DD, Pessoa AL, Franca GV, et al. The phenotypic spectrum of congenital Zika syndrome. Am J Med Genet A. 2017; 173:841–57.
6. Bonaldo MC, Ribeiro IP, Lima NS, Dos Santos AA, Menezes LS, da Cruz SO, et al. Isolation of infective Zika virus from urine and saliva of patients in Brazil. *PLoS Negl Trop Dis.* 2016;10: e0004816.
7. Shi W, Zhang Z, Ling C, Carr MJ, Tong Y, Gao GF. Increasing genetic diversity of Zika virus in the Latin American outbreak. Emerg Microbes Infect. 2016;5: e68.
8. Lindenbach BD, Rice CM. Molecular biology of flaviviruses. Adv Virus Res. 2003; 59:23–61.

9. Singh, R. K., Dhama, K., Malik, Y. S., Ramakrishnan, M. A., Karthik, K., Tiwari, R., Saurabh, S., Sachan, S., & Joshi, S. K. (2016). Zika virus – emergence, evolution, pathology, diagnosis, and control: Current global scenario and future perspectives – A comprehensive review. *Veterinary Quarterly*, *36*(3), 150–175. https://doi.org/10.1080/01652176.2016.1188333
10. Kaplowitz N, Aw TY, Ookhtens M. The regulation of hepatic GSH. *Ann Rev Pharm Toxicol.* 1985; 25:714–744.
11. Forman HJ, Zhang H, Rinna A. Glutathione: overview of its protective roles, measurement, and biosynthesis. *Mol Asp Med.* 2009;30:1–12.
12. Meredith MJ, Reed DJ. Status of the mitochondrial pool of glutathione in the isolated hepatocyte. *J Biol Chem.* 1982;257:3747–3753.
13. Yuan L, Kaplowitz N. Glutathione in liver diseases and hepatotoxicity. *Mol Asp Med.* 2009; 30:29–41.
14. Miranda-Filho D de B, Martelli CM, Ximenes RA, et al. Initial description of the presumed congenital Zika syndrome. Am J Public Health 2016; 106:598-600.
15. Duffy M.R., Chen T.H., Hancock W.T., Powers A.M., Kool J.L., Lanciotti R.S., Pretrick M., Marfel M., Holzbauer S., Dubray C., et al. Zika virus outbreak on Yap Island, Federated States of Micronesia. *N. Engl. J. Med.* 2009; 360:2536–2543. doi: 10.1056/NEJMoa0805715.
16. Rasmussen S.A., Jamieson D.J., Honein M.A., Petersen L.R. Zika Virus and Birth Defects—Reviewing the Evidence for Causality. *N. Engl. J. Med.* 2016; 374:1981–1987. doi: 10.1056/NEJMsr1604338.
17. Lu SC. Regulation of glutathione synthesis. *Mol Asp Med.* 2009; 30:42–59.

18. T.B. Deramaudt, C. Dill and M. Bonay Med. Mal. Infect., 43 (2013), pp. 100-107, 10.1016/j.medmal.2013.02.004

19. Almeida, L. T., Ferraz, A. C., da Silva Caetano, C. C., da Silva Menegatto, M. B., Dos Santos Pereira Andrade, A. C., Lima, R. L. S., Camini, F. C., Pereira, S. H., da Silva Pereira, K. Y., de Mello Silva, B., Perucci, L. O., Talvani, A., de Magalhães, J. C., & de Brito Magalhães, C. L. (2020). Zika virus induces oxidative stress and decreases antioxidant enzyme activities in vitro and in vivo. *Virus research*, *286*, 198084. https://doi.org/10.1016/j.virusres.2020.198084

20. Balakrishna, A., Krishna, P., Muthuraman, R., Mariappan, V., Srivatsan, S., 2019. Oxidative stress response in the pathogenesis of dengue virus virulence, disease prognosis and therapeutics: an update. Arch. Viro

21. Halliwell, B., Gutteridge, J.M.C., 2015. Free Radicals in Biology & Medicine. https://doi.

org/10.1017/CBO9781107415324.004.

22. Vasireddi, M., Crum, A., May, H., Katz, D., & Hilliard, J. (2019). A novel antiviral inhibits Zika virus infection while increasing intracellular glutathione biosynthesis in distinct cell culture models. *Antiviral research*, *161*, 46–52. https://doi.org/10.1016/j.antiviral.2018.09.004

23. Itoh, K., Wakabayashi, N., Katoh, Y., Ishii, T., O'Connor, T., and Yamamoto, M. (2003) Keap1 regulates both cytoplasmic-nuclear shuttling and degradation of Nrf2 in response to electrophiles, *Genes Cells 8*, 379-391.

24. McMahon, M., Itoh, K., Yamamoto, M., and Hayes, J. D. (2003) Keap1-dependent proteasomal degradation of transcription factor Nrf2 contributes to the negative regulation of antioxidant response element-driven gene expression, *J. Biol. Chem. 278*, 21592- 21600.

25. Kobayashi, A., Kang, M. I., Okawa, H., Ohtsuji, M., Zenke, Y., Chiba, T., Igarashi, K., and Yamamoto, M. (2004) Oxidative stress sensor Keap1 functions as an adaptor for Cul3-based E3 ligase to regulate proteasomal degradation of Nrf2, *Mol. Cell. Biol. 24*, 7130-7139.

26. Hayes, J. D., & Dinkova-Kostova, A. T. (2014). The Nrf2 regulatory network provides an interface between redox and intermediary metabolism. *Trends in Biochemical Sciences*, *39*(4), 199–218. https://doi.org/10.1016/j.tibs.2014.02.002

27. Beutler, T.M., Gallagher, E.P., Wang, C., Stahl, D.L., Hayes, J.D. & Eaton, D.L. (1995) Induction of phase I and phase II drug metabolizing enzyme mRNA, protein and activity by BHA, ethoxyquin and oltipraz. *Toxicol. Appl. Pharmacol.* **135**, 45– 57.

28. Friling, R.S., Bensimon, S. & Daniel, V. (1990) Xenobiotic-inducible expression of murine glutathione S-transferase Ya subunit gene is controlled by an electrophile-responsive element. *Proc. Natl. Acad. Sci. USA* **87**, 6258– 6262.

29. Hayes, J.D. & Pulford, J.D. (1995) The glutathione S-transferase supergene family: Regulation of GST and the contribution of the isozymes to cancer chemoprevention and drug resistance. *Crit. Rev. Biochem. Mol. Biol.* **30**, 445– 600.

30. Prestera, T., Zhang, Y., Spencer, R.S., Wilczak, A.C. & Talalay, P. (1993) The electrophile counterattack response: protection against neoplasia and toxicity. *Adv. Enzyme Regul.* **33**, 281– 296.

31. Primiano, T., Sutter, T.R. & Kensler, T.W. (1997) Antioxidant-inducible genes. *Adv. Pharmacol.* **38**, 293– 328.

32. D'Autreaux B, Toledano MB. ROS as signalling molecules: mechanisms that generate specificity in ROS homeostasis. Nat Rev Mol Cell Biol. 2007;8(10):813–24.

33. Ray, P. D., Huang, B. W., & Tsuji, Y. (2012). Reactive oxygen species (ROS) homeostasis and redox regulation in cellular signaling. *Cellular signalling*, *24*(5), 981–990. https://doi.org/10.1016/j.cellsig.2012.01.008

34. Jakubczyk, K., Dec, K., Kałduńska, J., Kawczuga, D., Kochman, J., & Janda, K. (2020). Reactive oxygen species - sources, functions, oxidative damage. *Polski merkuriusz lekarski : organ Polskiego Towarzystwa Lekarskiego*, *48*(284), 124–127.

35. Dröge W. Free radicals in the physiological control of cell function. *Physiological Reviews.* 2002;82(1):47–95. doi: 10.1152/physrev.00018.2001.

36. Li, B., Li, X., Zhu, B., Zhang, X., Wang, Y., Xu, Y., Wang, H., Hou, Y., Zheng, Q., & Sun, G. (2013). Sodium arsenite induced reactive oxygen species generation, nuclear factor (erythroid-2 related) factor 2 activation, heme oxygenase-1 expression, and glutathione elevation in Chang human hepatocytes. *Environmental toxicology*, *28*(7), 401–410. https://doi.org/10.1002/tox.20731

37. Almeida, L. T., Ferraz, A. C., da Silva Caetano, C. C., da Silva Menegatto, M. B., dos Santos Pereira Andrade, A. C., Lima, R. L., Camini, F. C., Pereira, S. H., da Silva Pereira, K. Y., de Mello Silva, B., Perucci, L. O., Talvani, A., de Magalhães, J. C., & de Brito Magalhães, C. L. (2020). Zika virus induces oxidative stress and decreases antioxidant enzyme activities in vitro and in vivo. *Virus Research*, *286*, 198084. https://doi.org/10.1016/j.virusres.2020.198084

38. Lee, C. (2018). Therapeutic modulation of virus-induced oxidative stress via the Nrf2-dependent antioxidative pathway. *Oxidative Medicine and Cellular Longevity*, *2018*.

39. Baird, L., & Yamamoto, M. (2020). The Molecular Mechanisms Regulating the KEAP1-NRF2 Pathway. *Molecular and cellular biology*, *40*(13), e00099-20. https://doi.org/10.1128/MCB.00099-20

40. Ramezani, A., Nahad, M. P., & Faghihloo, E. (2018). The role of NRF2 transcription factor in viral infection. *Journal of Cellular Biochemistry*, *119*(8), 6366–6382. https://doi.org/10.1002/jcb.26897

41. Saha, S., Buttari, B., Panieri, E., Profumo, E., & Saso, L. (2020). An Overview of Nrf2 Signaling Pathway and Its Role in Inflammation. *Molecules (Basel, Switzerland)*, *25*(22), 5474. https://doi.org/10.3390/molecules25225474

42. Yamamoto, M., Kensler, T. W., & Motohashi, H. (2018). The KEAP1-NRF2 System: a Thiol-Based Sensor-Effector Apparatus for Maintaining Redox Homeostasis. *Physiological reviews*, *98*(3), 1169–1203. https://doi.org/10.1152/physrev.00023.2017.

43. Munjal, A., Khandia, R., Dhama, K., Sachan, S., Karthik, K., Tiwari, R., Malik, Y. S., Kumar, D., Singh, R. K., Iqbal, H. M. N., & Joshi, S. K. (2017). Advances in Developing Therapies to Combat Zika Virus: Current Knowledge and Future Perspectives. *Frontiers in microbiology*, *8*, 1469. https://doi.org/10.3389/fmicb.2017.01469

44. Ramezani, A., Nahad, M. P., & Faghihloo, E. (2018a). The role of NRF2 transcription factor in viral infection. *Journal of Cellular Biochemistry*, *119*(8), 6366–6382. https://doi.org/10.1002/jcb.26897

45. Ramezani, A., Nahad, M. P., & Faghihloo, E. (2018). The role of NRF2 transcription factor in viral infection. *Journal of Cellular Biochemistry*, *119*(8), 6366–6382. https://doi.org/10.1002/jcb.26897